

Measurement of Ξ_c^+ production in p Pb collisions at $\sqrt{s_{NN}} = 8.16$ TeV at LHCbR. Aaij *et al.**
(LHCb Collaboration)

(Received 17 May 2023; revised 6 November 2023; accepted 11 January 2024; published 1 April 2024)

A study of prompt Ξ_c^+ production in proton-lead collisions is performed with the LHCb experiment at a center-of-mass energy per nucleon pair of 8.16 TeV in 2016 in p Pb and Pb p collisions with an estimated integrated luminosity of approximately 12.5 and 17.4 nb⁻¹, respectively. The Ξ_c^+ production cross section, as well as the Ξ_c^+ to Λ_c^+ production cross-section ratio, are measured as a function of the transverse momentum and rapidity and compared to the latest theory predictions. The forward-backward asymmetry is also measured as a function of the Ξ_c^+ transverse momentum. The results provide strong constraints on theoretical calculation and are a unique input for hadronization studies in different collision systems.

DOI: [10.1103/PhysRevC.109.044901](https://doi.org/10.1103/PhysRevC.109.044901)**I. INTRODUCTION**

In hadronic collisions, heavy quarks are produced in hard scattering processes with large momentum transfer. Theoretical predictions based on perturbative quantum chromodynamics (pQCD) describe reasonably well the transverse momentum (p_T) differential charm production cross sections in proton-proton (pp) collisions at different energies [1]. The heavy-flavor hadron cross sections are usually computed using the factorization approach as a convolution of three terms [2]: the parton distribution functions of the colliding particles, the hard-scattering cross section, and the fragmentation function (FF) of heavy quarks into a given heavy-flavor hadron. It is assumed that the FFs are universal between collision systems and energies. At the CERN Large Hadron Collider (LHC), the FFs used to describe the measurements of heavy-flavor hadron production in pp collisions at different center-of-mass energies are tuned on e^+e^- collision data within the framework of pQCD over a wide p_T range. However, evidence of nonuniversal FFs was observed by the LHCb collaboration in a study of the Λ_b^0 baryon to B^- and \bar{B}^0 meson production ratio in pp collisions [3]. Multiple measurements of the relative production of different heavy-flavor hadron species have been made, as they are sensitive probes of FFs.

The measurements of heavy-flavored hadron ratios in hadronic collisions, such as the Λ_c^+/D^0 cross-section ratio, in pp collisions at $\sqrt{s} = 5, 7,$ and 13 TeV and in proton-lead (p Pb) collisions at $\sqrt{s} = 5$ TeV [4–6], show an enhancement with respect to predictions from pQCD calculations

with charm fragmentation based on e^+e^- [7,8] and e^-p [9–11] measurements. Similar observations were made in the measurement of the $\Xi_c^0(\Xi_c^+)/D^0$ cross-section ratio in pp collisions at $\sqrt{s} = 7$ and 13 TeV [12,13]. Multiple models explain the ratio enhancement. For example, color reconnection [14] could be stronger in pp collisions than in e^+e^- collisions, resulting in an enhanced production of baryons relative to mesons. Other models predicts that hadronization via coalescence [15] will take place.

This paper presents a study of the ratio of production of the Ξ_c^+ particle, a charm-strange baryon, to the production of the Λ_c^+ baryon in p Pb collisions at the LHCb experiment. This measurement has the potential to shed light on the mechanism of hadronization and its universality as it is the first one to be performed in proton-nucleus collisions, considered the best environment to study the so-called cold nuclear matter (CNM) effects, such as shadowing [16–18], energy loss [19], and nuclear break-up [20]. In nucleus-nucleus collisions, in addition to CNM effects, experimental results indicate the formation of a high-density color-deconfined medium, the quark-gluon plasma (QGP), a state of matter with asymptotically free partons, which is expected to exist at extremely high temperature and density. The presence of QGP can be determined by observing the change in behavior of the particles as they traverse the nuclear medium with respect to their behavior in the absence of QGP [21]. In p Pb collisions the energy density is not expected to be sufficient to produce a QGP medium; however, some theoretical models predict the formation of “QGP droplets” [22], which could partially induce in p Pb the same behavior, albeit less pronounced, as in PbPb collisions. Moreover, several QGP models predict that strange (s) quark production is enhanced in heavy-ion collisions, as first reported in Ref. [23]; thus, strangeness enhancement and strange antibaryon abundance are considered signatures for QGP formation [24–26], mainly due to the predominance of the gluonic production mechanism $gg \rightarrow s\bar{s}$. Strangeness enhancement is investigated at accelerators by studying the ratio of production rates of hadrons containing a strange quark

*Full author list given at the end of the article.

Published by the American Physical Society under the terms of the [Creative Commons Attribution 4.0 International](https://creativecommons.org/licenses/by/4.0/) license. Further distribution of this work must maintain attribution to the author(s) and the published article's title, journal citation, and DOI. Funded by SCOAP³.

to those without, as done, by experiments at CERN [27] and BNL Relativistic Heavy Ion Collider (RHIC) [28,29]. The ratio of Ξ_c^+ to Λ_c^+ production measured in this paper, by comparing a baryon with strange content to one without, has the potential to test the presence of QGP formation from QGP droplets in p Pb collisions, which has not yet been established.

II. ANALYSIS, DETECTOR, AND SIMULATION

The Ξ_c^+ and Λ_c^+ candidates¹ in the analysis are reconstructed via the hadronic decay to the $pK^-\pi^+$ final state. The measurements are performed as a function of p_T and rapidity (y^*) of the baryons, using p Pb and Pb p collisions with an estimated integrated luminosity of approximately 12.5 and 17.4 nb^{-1} [30], respectively, collected by the LHCb detector at center-of-mass energy per nucleon pair of $\sqrt{s_{NN}} = 8.16$ TeV. The rapidity y^* in the nucleon-nucleon center-of-mass system is related to the rapidity in the laboratory frame (y_{lab}) via $y^* = y_{\text{lab}} \pm 0.4645$. Here, 0.4645 is the shift in rapidity in the direction of the proton beam due to the unequal mass of the two colliding objects. The proton beam and the lead beam have different energies per nucleon in the laboratory frame, with $E_p = 6.5$ TeV and $E_{\text{Pb}} = 2.56$ TeV. The particles are separated according to whether they originate from the collision point (prompt) or from the decay of b hadrons (nonprompt) using the impact parameter (IP), defined as the distance of closest approach of the particle trajectory to the collision point. Data are analyzed separately in the p Pb (forward) sample, covering a rapidity range $1.5 < y^* < 4.0$, and the Pb p (backward) sample, covering the range $-5.0 < y^* < -2.5$.

The double differential cross section for prompt Ξ_c^+ (Λ_c^+) production is measured as

$$\frac{d^2\sigma_{\Xi_c^+(\Lambda_c^+)}(p_T, y^*)}{dp_T dy^*} = \frac{N_{\Xi_c^+(\Lambda_c^+)}(p_T, y^*)}{\mathcal{L} \cdot \mathcal{B} \cdot \epsilon_{\text{tot}}(p_T, y^*) \cdot \Delta p_T \Delta y^*}, \quad (1)$$

where $N_{\Xi_c^+(\Lambda_c^+)}(p_T, y^*)$ is the measured signal yield of prompt Ξ_c^+ (Λ_c^+) decays produced in a given interval of p_T and y^* , Δp_T and Δy^* , respectively, and \mathcal{L} represents the integrated luminosity. The branching fractions \mathcal{B} are $(0.62 \pm 0.30)\%$ and $(6.28 \pm 0.32)\%$, for the decays $\Xi_c^+ \rightarrow pK^-\pi^+$ and $\Lambda_c^+ \rightarrow pK^-\pi^+$, respectively [31]. Finally, $\epsilon_{\text{tot}}(p_T, y^*)$ stands for the total signal efficiency determined in the Δp_T and Δy^* interval. The production ratio of Ξ_c^+ to Λ_c^+ , $R_{\Xi_c^+/\Lambda_c^+}(p_T, y^*)$, is defined as

$$R_{\Xi_c^+/\Lambda_c^+}(p_T, y^*) \equiv \frac{d^2\sigma_{\Xi_c^+}(p_T, y^*)/dp_T dy^*}{d^2\sigma_{\Lambda_c^+}(p_T, y^*)/dp_T dy^*}. \quad (2)$$

The forward-backward asymmetry, $R_{\text{FB}}(p_T, y^*)$, is measured in the overlapping rapidity range $2.5 < |y^*| < 4.0$ and is defined as

$$R_{\text{FB}}(p_T, y^*) \equiv \frac{d^2\sigma_{\Xi_c^+}(p_T, +|y^*|)/dp_T dy^*}{d^2\sigma_{\Xi_c^+}(p_T, -|y^*|)/dp_T dy^*}. \quad (3)$$

The LHCb detector [32,33] is a single-arm forward spectrometer covering the pseudorapidity range $2 < \eta < 5$, designed for the study of particles containing b or c quarks. The detector includes a high-precision tracking system consisting of a silicon-strip vertex detector surrounding the pp interaction region [34], a large-area silicon-strip detector located upstream of a dipole magnet with a bending power of about 4 Tm, and three stations of silicon-strip detectors and straw drift tubes [35] placed downstream of the magnet. The tracking system provides a measurement of the momentum, p , of charged particles with a relative uncertainty that varies from 0.5% at low momentum to 1.0% at 200 GeV/ c . The minimum distance of a track to a primary pp collision vertex (PV), the impact parameter (IP), is measured with a resolution of $(15 + 29/p_T)\mu\text{m}$, where p_T is the component of the momentum transverse to the beam, in GeV/ c . The different types of charged hadrons, such as the kaons and pions used in this analysis, are distinguished using information from two ring-imaging Cherenkov detectors [36]. Photons, electrons and hadrons are identified by a calorimeter system consisting of scintillating-pad and preshower detectors, an electromagnetic and a hadronic calorimeter. Muons are identified by a system composed of alternating layers of iron and multiwire proportional chambers [37]. The online event selection is performed by a trigger [38], which consists of a hardware stage, based on information from the calorimeter and muon systems, followed by a software stage, which applies a full event reconstruction.

Simulation is used to model the reconstruction efficiency and the effects of the selection requirements. Charmed baryons are generated in pp collisions at $\sqrt{s} = 8.16$ TeV using the PYTHIA [39] generator and are embedded into the EPOS [40] generator, which simulates the environment of the proton-lead collision. Particle decays are described by EVTGEN [41], while the interaction of particles with the detector, and its response in simulation, are implemented using the GEANT4 toolkit [42,43].

III. CANDIDATE SELECTION

The online event selection is performed by a trigger, which consists of a hardware stage followed by a two-level software stage. In between the two software stages, an alignment and calibration of the detector is performed in near real-time and their results are used in the trigger [44]. The same alignment and calibration information is propagated to the offline reconstruction, ensuring consistent and high-quality particle identification (PID) information between the trigger and offline software. The identical performance of the online and offline reconstruction offers the opportunity to perform physics analyses directly using candidates reconstructed in the trigger [38,45] which the present analysis exploits. The Ξ_c^+ and Λ_c^+ baryons are reconstructed by combining three tracks identified as proton, kaon, and pion candidates. All the charged tracks are required to be well reconstructed and to have transverse momentum $p_T > 400$ MeV/ c and be incompatible with originating at the PV. The tracks must also be within the LHCb acceptance $2.0 < \eta < 5.0$ and in the kinematic range $3.2 < p < 100.0$ GeV/ c . The Ξ_c^+ and Λ_c^+

¹Charge conjugate decays are implied throughout this paper, unless otherwise stated.

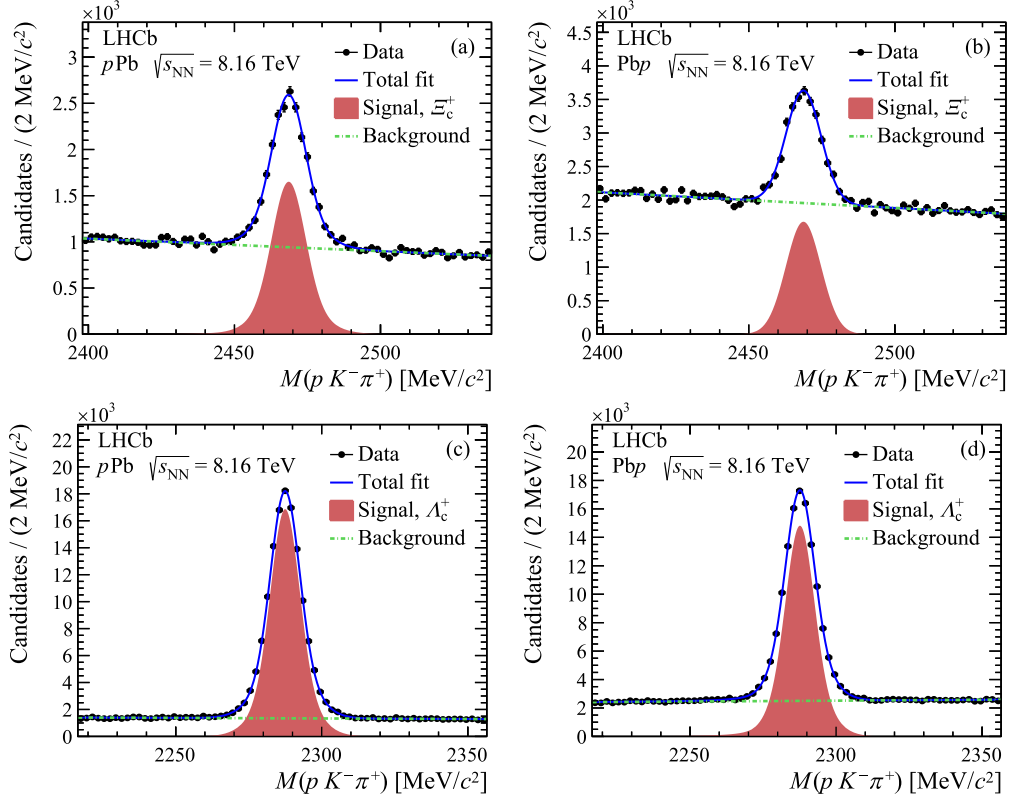


FIG. 1. Invariant mass distributions for (a) Ξ_c^+ candidates in $p\text{Pb}$ data, (b) Ξ_c^+ candidates in $\text{Pb}p$ data, (c) Λ_c^+ candidates in $p\text{Pb}$ data, and (d) Λ_c^+ candidates in $\text{Pb}p$ data. The results of the fit are overlaid.

candidates are required to have a good quality secondary vertex and a reconstructed decay time between 0.1 and 10 ps. The angle between the reconstructed candidate momentum and the vector pointing from the PV to the secondary vertex is required to be close to zero. The $pK^-\pi^+$ invariant mass is required to be within ± 70 MeV/c^2 of the known Ξ_c^+ (Λ_c^+) mass [31]. The invariant mass resolution for the reconstructed candidates is around 10 MeV/c^2 .

IV. DETERMINATION OF SIGNAL YIELDS AND EFFICIENCY

The signal yields are determined using a maximum-likelihood fit to the $pK^-\pi^+$ invariant mass distributions, which were verified to be independent of the other kinematic variables. The signal component of the fit model is represented by a sum of a Crystal Ball function [46] and a Gaussian function, which share a common mean value. The background component is described by a linear function. The results of the invariant mass fits for Ξ_c^+ and Λ_c^+ in $p\text{Pb}$ and $\text{Pb}p$ data samples are shown in Fig. 1.

The obtained signal yields are about 13.3×10^3 (12.6×10^3) Ξ_c^+ decays and 119.2×10^3 (104.4×10^3) Λ_c^+ decays in the $p\text{Pb}$ ($\text{Pb}p$) sample after background subtraction, achieved using the *sPlot* technique [47] with the $pK^-\pi^+$ invariant mass as the discriminating variable. The extracted signal contains promptly produced baryons and nonprompt signal from the

decay of b hadrons. To extract the prompt component, the method developed in Ref. [6] is used, with the variable χ_{IP}^2 discriminating between prompt and nonprompt production. The χ_{IP}^2 variable is defined as the difference in the vertex-fit χ^2 of a given PV reconstructed with and without the Ξ_c^+ (Λ_c^+) candidate under consideration. The prompt and nonprompt components are modelled with a Bukin function [48]. The asymmetry parameters of the Bukin function describing the prompt component are fixed using results from fits to simulated samples. The results of the background-subtracted distribution fits of the $\log_{10}(\chi_{\text{IP}}^2)$ for Ξ_c^+ and Λ_c^+ in $p\text{Pb}$ and $\text{Pb}p$ data samples are shown in Fig. 2. The quantity $N^{\Xi_c^+ (\Lambda_c^+)}(p_T, y^*)$ is obtained by performing the invariant mass and $\log_{10}(\chi_{\text{IP}}^2)$ fits in each (p_T, y^*) bin.

Simulated data are used to determine the total efficiency, defined as the product of the geometrical acceptance of the detector, and the reconstruction, selection, PID, and trigger efficiencies. The samples are weighted to match the background-subtracted data using the distributions of p_T , y^* , the number of VELO clusters and the invariant mass of the pK^- and $K^-\pi^+$ combinations. The PID efficiency is also measured with dedicated calibration data samples [49].

V. SYSTEMATIC UNCERTAINTIES

Several sources of systematic uncertainty are studied. A systematic uncertainty in the signal yield determination is

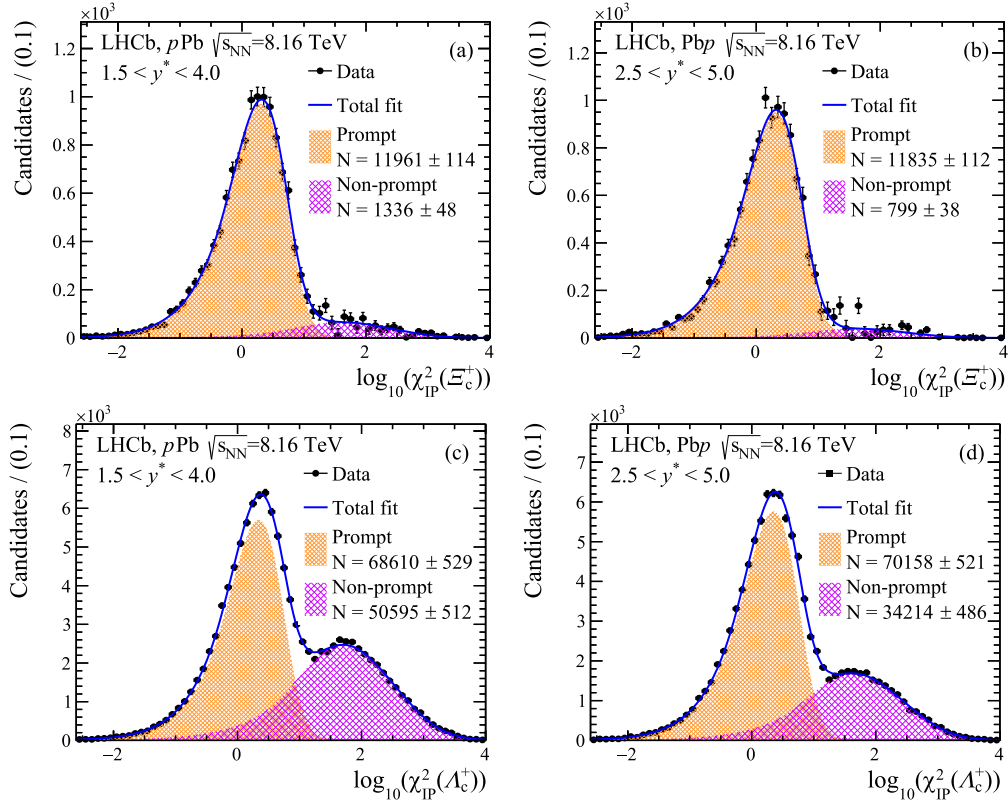


FIG. 2. Background-subtracted $\log_{10}(\chi_{\text{IP}}^2)$ distributions of (a) Ξ_c^+ and (b) Λ_c^+ candidates in (left) $p\text{Pb}$ and (right) $\text{Pb}p$ data. The results of the fit are overlaid.

evaluated by changing the function used in the fit for the nonprompt component, switching from a Bukin function to a Gaussian. The difference in the signal yields obtained with the two fits is taken as a systematic uncertainty. The systematic uncertainty associated to the background determination, which is dominant, is evaluated by using a sideband subtraction technique, instead of the $sPlot$ method. The uncertainties in reconstruction, selection, and PID efficiencies are evaluated by varying the reweighting procedure by excluding the distributions of the invariant mass of the pK^- and $K^-\pi^+$ combinations. The uncertainties in the branching fractions are accounted for. Summaries of the systematic uncertainties in

TABLE I. Summary of systematic uncertainties on the Ξ_c^+ and Λ_c^+ cross sections in p_T bins in the $p\text{Pb}$ and $\text{Pb}p$ samples. The range of uncertainties correspond to the values obtained for different bins of p_T .

	Ξ_c^+		Λ_c^+	
	$p\text{Pb}$	$\text{Pb}p$	$p\text{Pb}$	$\text{Pb}p$
Signal	0.1–2.2%	0.2–2.3%	–	–
Background	1.3–5.7%	0.5–18.0%	0.1–1.0%	0.1–0.8%
ε_{acc}	0.1–0.2%	0.1–0.3%	0.1–0.2%	0.1–0.2%
$\varepsilon_{\text{sel/rec}}$	1.1–3.5%	1.3–4.8%	3.6–7.3%	2.7–5.5%
ε_{PID}	0.3–0.7%	0.6–1.4%	0.2–0.6%	0.5–1.1%
$\varepsilon_{\text{trg/sel}}$	0.4–0.5%	0.4–0.5%	0.1–0.6%	0.4–0.8%
Total	2.0–6.3%	2.9–18.0%	3.6–7.3%	2.8–5.6%

the Ξ_c^+ and Λ_c^+ cross sections can be found in Tables I, II, and III.

VI. RESULTS

In this section the different measurements performed are discussed. More results can be found in the Appendix.

A. Double-differential cross section

The double-differential cross sections of prompt Ξ_c^+ production times $\mathcal{B}(\Xi_c^+ \rightarrow pK^-\pi^+)$ in proton-lead collisions at

TABLE II. Summary of systematic uncertainties on the Ξ_c^+ and Λ_c^+ cross sections in y^* bins in the $p\text{Pb}$ and $\text{Pb}p$ samples. The range of uncertainties correspond to the values obtained for different bins of y^* .

	Ξ_c^+		Λ_c^+	
	$p\text{Pb}$	$\text{Pb}p$	$p\text{Pb}$	$\text{Pb}p$
Signal	0.2–3.0%	0.2–3.6%	2.0–5.9%	–
Background	0.1–5.7%	1.7–27.4%	0.1–4.6%	0.7–17.7%
ε_{acc}	0.1–0.4%	0.1–0.8%	0.1–0.3%	0.1–0.5%
$\varepsilon_{\text{sel/rec}}$	0.7–2.8%	1.5–4.2%	3.4–6.8%	1.2–14.4%
ε_{PID}	0.4–1.5%	0.5–3.0%	0.2–2.3%	0.4–3.8%
$\varepsilon_{\text{trg/sel}}$	0.4–0.5%	0.4–0.6%	0.4–0.5%	0.4–1.2%
Total	1.6–6.4%	2.7–27.8%	4.1–9.9%	1.8–17.9%

TABLE III. Summary of systematic uncertainties correlated among bins on the Ξ_c^+ and Λ_c^+ cross sections in the $p\text{Pb}$ and $\text{Pb}p$ samples.

	$p\text{Pb}$	$\text{Pb}p$
Luminosity	2.6%	2.5%
Signal	4.8%	2.8–3.1%
Tracking		5.5%
$\mathcal{B}(\Xi_c^+ \rightarrow p^+ K^- \pi^+)$		48.4%
$\mathcal{B}(\Lambda_c^+ \rightarrow p^+ K^- \pi^+)$		5.1%

$\sqrt{s_{NN}} = 8.16$ TeV are measured as a function of p_T integrated over y^* in the regions $1.5 < y^* < 4.0$ and $-5.0 < y^* < -2.5$, and as a function of y^* integrated over the p_T range between 2.0 and 12.0 GeV/c. The double-differential cross sections of prompt Ξ_c^+ production are shown in Fig. 3. The data are compared with theoretical predictions [50–52] from

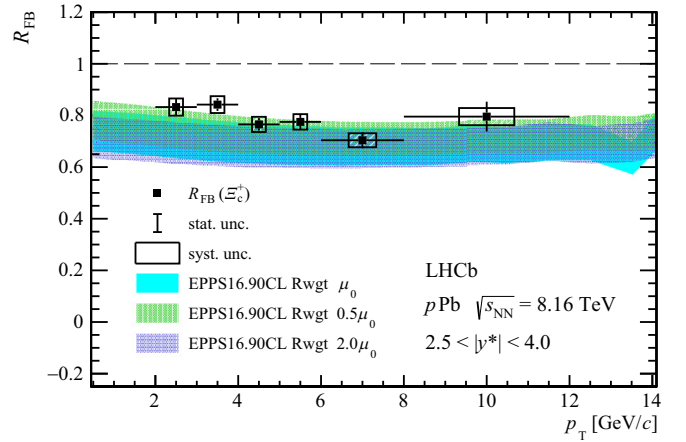


FIG. 4. Forward-backward ratio of Ξ_c^+ production as a function of p_T . The error bars represent the statistical uncertainties, while the boxes indicate the systematic uncertainty.

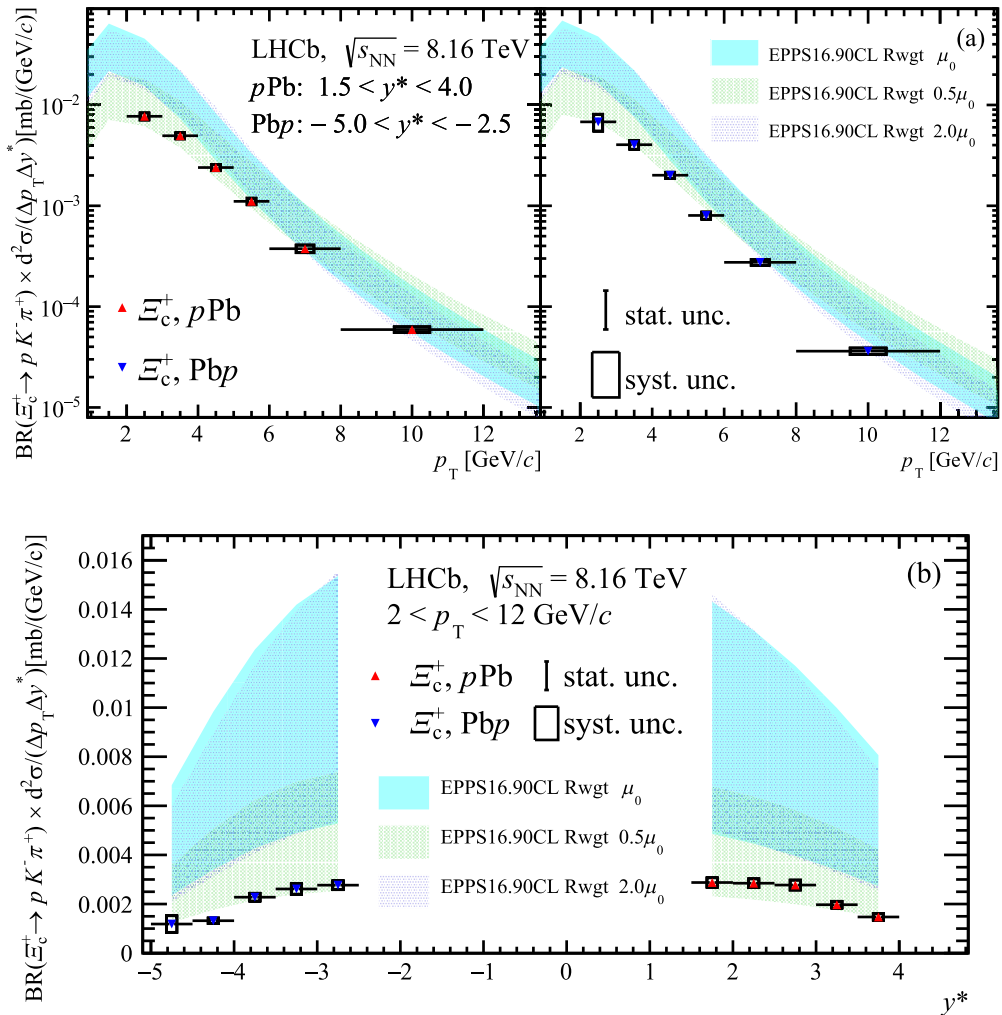


FIG. 3. Double-differential cross-section of the prompt Ξ_c^+ baryon times $\mathcal{B}(\Xi_c^+ \rightarrow pK^-\pi^+)$ in proton-lead collisions as a function of (a) p_T and (b) y^* in $p\text{Pb}$ (red triangles) and $\text{Pb}p$ (blue triangles) collisions. The error bars represent the statistical uncertainties, while the black squares represent the total systematic uncertainties which include correlations among bins.

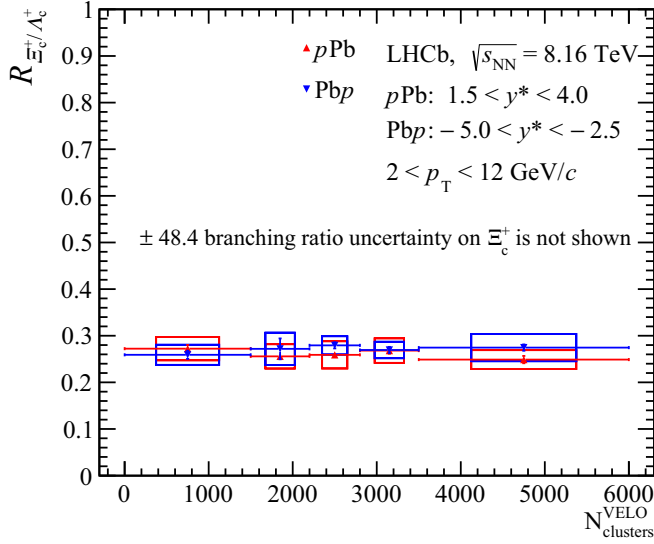
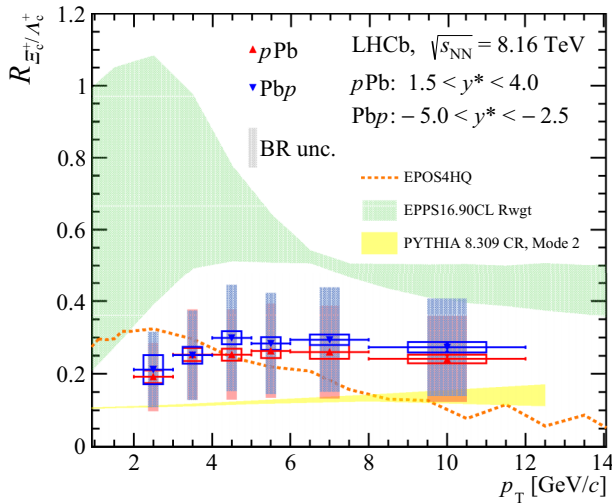


FIG. 5. Ratio of prompt Ξ_c^+ to Λ_c^+ production in *pPb* (red triangles) and *Pb p* (blue triangles) data samples as a function of $N_{clusters}^{VELO}$. The error bars represent the statistical uncertainties, while the squares indicate the systematic uncertainty. The branching ratio uncertainty on Ξ_c^+ is not shown.

the HELAC-Onia method [53,54] called EPPS16 [55] with three factorization scale choices. The data agree with the predictions and appear to be best described using the scale $0.5\mu_0$. For the forward and backward regions, the integrated cross sections are

$$\begin{aligned} \sigma_{\Xi_c^+}^{pPb}(2 < p_T < 12 \text{ GeV}/c, 1.5 < y^* < 4.0) \\ &= 9.69 \pm 0.12 \pm 0.26 \pm 4.72 \text{ mb}, \\ \sigma_{\Xi_c^+}^{Pb p}(2 < p_T < 12 \text{ GeV}/c, -5.0 < y^* < -2.5) \\ &= 8.10 \pm 0.11 \pm 0.72 \pm 3.95 \text{ mb}, \end{aligned}$$



where the first uncertainty is statistical, the second is the uncorrelated systematic uncertainty, and the third is the systematic uncertainty fully correlated among bins.

B. Forward-backward asymmetry

The forward-backward ratio R_{FB} , defined in Eq. (3) and measured as a function of p_T , is shown in Fig. 4. The ratio is independent of p_T and agrees with the theoretical prediction within one standard deviation.

C. Differential ratio of Ξ_c^+ to Λ_c^+ (D^0)

The differential ratio of Ξ_c^+ to Λ_c^+ production is measured as a function of the number of clusters reconstructed in the VELO ($N_{clusters}^{VELO}$) and given in Fig. 5. The ratios are constant as a function of $N_{clusters}^{VELO}$, similarly for the *pPb* and *Pb p* data, and the results show no indication of strangeness enhancement.

Since LHCb has already measured the D^0 production cross-section in *pPb* collisions at $\sqrt{s} = 8.16$ TeV [56], it is also possible to compute the Ξ_c^+/D^0 production ratio. The differential ratios of Ξ_c^+ to Λ_c^+ production and Ξ_c^+ to D^0 production are shown in Fig. 6 as a function of p_T . Both the Ξ_c^+/Λ_c^+ and Ξ_c^+/D^0 ratios show no significant p_T dependence, similarly for the *pPb* and *Pb p* data samples. This result provides a strong indication that the same processes govern hadronization in *pPb* and *Pb p* collisions. This is the first time they are measured in this system. The data are compared with EPPS16 nPDF predictions [55], which uses the cross section measured in *pp* collisions by ALICE [13] as input for their calculation. The EPPS16 model shows a similar trend as the data, but significantly overestimates it. The measurements are also compared with results from the PYTHIA 8.3 event generator with a tune that implements color reconnection (CR) beyond the leading-colour approximation [14] and the computation obtained with EPOS4HQ, the heavy quark extension of the new EPOS4 framework [4]. Both computations are based on results in *pp* collisions. The Ξ_c^+/Λ_c^+

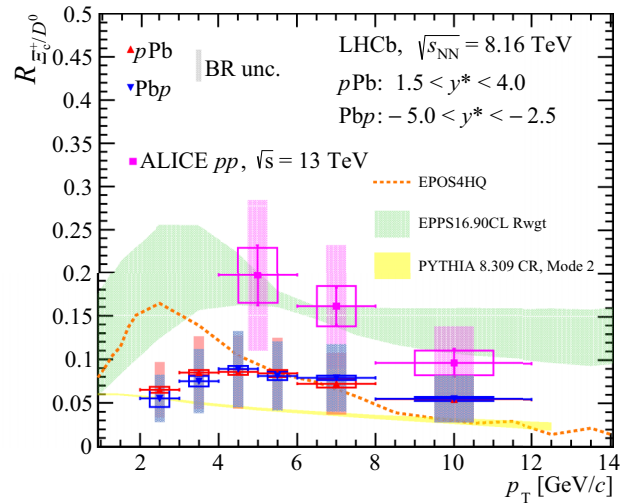


FIG. 6. Ratio of (left) prompt Ξ_c^+ to Λ_c^+ production and (right) Ξ_c^+ to D^0 production in the *pPb* (red triangles) and *Pb p* (blue triangles) data samples as a function of p_T . The error bars represent the statistical uncertainties, while the empty rectangles indicate the systematic uncertainty. Shaded rectangles denote the branching ratio uncertainty.

cross-section ratio is best described by the EPOS4HQ model within uncertainties, despite showing a different trend, especially at low p_T . This behavior is even more pronounced in the Ξ_c^+/D^0 cross-section ratio. The Ξ_c^+ to D^0 production ratio is also compared with the result of ALICE at $\sqrt{s} = 13$ TeV at $|y| < 0.5$ in pp collisions [13]. The ALICE result is generally higher, but the two measurements agree within the uncertainties.

VII. SUMMARY

In summary, the prompt Ξ_c^+ production cross section in $p\text{Pb}$ and $\text{Pb}p$ collisions at a center-of-mass energy of $\sqrt{s_{NN}} = 8.16$ TeV at the LHCb experiment is measured differentially for the first time as a function of p_T and y^* . The cross-section measurement provides new constraints for nPDF calculations, especially at low p_T , where the uncertainty on the factorization scale is the largest. The forward-backward ratio R_{FB} is measured and found to be well described by nuclear shadowing calculations showing that there are no major final-state effects involved, in contrast to what has been observed in D^0 production studies in the same kinematic range at the same energy [56]. Prompt Ξ_c^+ production is compared to prompt Λ_c^+ production in the same kinematic region and their ratio is found to be constant within the uncertainties as a function of p_T and multiplicity, which is an indication that similar effects govern both Ξ_c^+ and Λ_c^+ production. The ratio of Ξ_c^+ to D^0 production is also measured as a function of p_T . Both ratios are found to be similar in $p\text{Pb}$ and $\text{Pb}p$ collisions but they show different trends compared to pp theory calculations. Therefore, our results show that hadronization in $p\text{Pb}$ is not well understood and

provides clear input for the hadronization studies in $p\text{Pb}$ collisions.

ACKNOWLEDGMENTS

We would like to thank to Hua-Sheng Shao, Jiaxing Zhao, and Joerg Aichelin for providing LHCb-specific theoretical predictions. We express our gratitude to our colleagues in the CERN accelerator departments for the excellent performance of the LHC. We thank the technical and administrative staff at the LHCb institutes. We acknowledge support from CERN and from the national agencies: CAPES, CNPq, FAPERJ, and FINEP (Brazil); MOST and NSFC (China); CNRS/IN2P3 (France); BMBF, DFG, and MPG (Germany); INFN (Italy); NWO (Netherlands); MNiSW and NCN (Poland); MCID/IFA (Romania); MICINN (Spain); SNSF and SER (Switzerland); NASU (Ukraine); STFC (United Kingdom); DOE NP and NSF (USA). We acknowledge the computing resources that are provided by CERN, IN2P3 (France), KIT and DESY (Germany), INFN (Italy), SURF (Netherlands), PIC (Spain), GridPP (United Kingdom), CSCS (Switzerland), IFIN-HH (Romania), CBPF (Brazil), and Polish WLCG (Poland). We are indebted to the communities behind the multiple open-source software packages on which we depend. Individual groups or members have received support from ARC and ARDC (Australia); Key Research Program of Frontier Sciences of CAS, CAS PIFI, CAS CCEPP, Fundamental Research Funds for the Central Universities, and Sci. & Tech. Program of Guangzhou (China); Minciencias (Colombia); EPLANET, Marie Skłodowska-Curie Actions, ERC and NextGenerationEU (European Union); A*MIDEX, ANR, IPhU and Labex P2IO, and Région Auvergne-Rhône-Alpes (France); AvH Foundation (Germany); ICSC

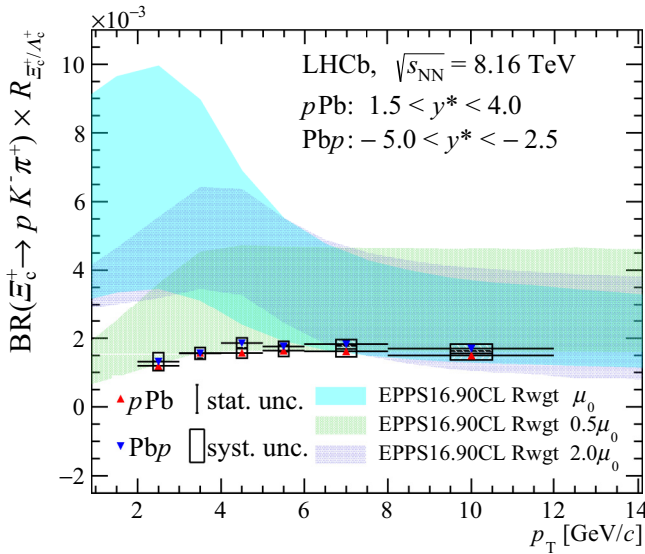


FIG. 7. Production ratio of prompt Ξ_c^+ to Λ_c^+ baryons multiplied by $\mathcal{B}(\Xi_c^+ \rightarrow pK^-\pi^+)$ in $p\text{Pb}$ (red triangles) and $\text{Pb}p$ (blue triangles) data samples as a function of p_T . The error bars represent the statistical uncertainties while the squares indicate the systematic uncertainty.

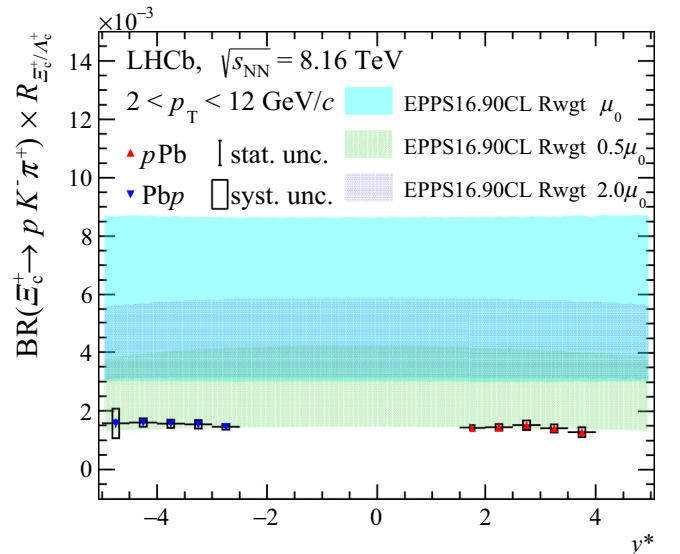


FIG. 8. Production ratio of prompt Ξ_c^+ to Λ_c^+ baryons multiplied by $\mathcal{B}(\Xi_c^+ \rightarrow pK^-\pi^+)$ in $p\text{Pb}$ (red triangles) and $\text{Pb}p$ (blue triangles) data samples as a function of y^* . The error bars represent the statistical uncertainties while the squares indicate the systematic uncertainty.

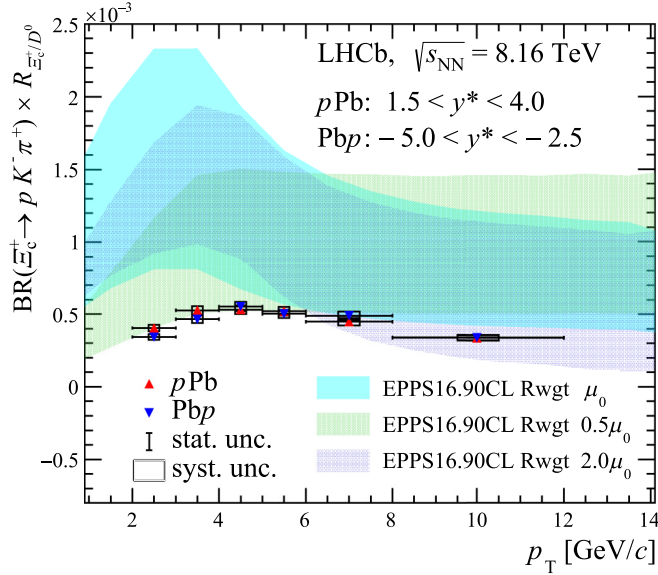


FIG. 9. Production ratio of prompt Ξ_c^+ to D^0 baryons multiplied by $\mathcal{B}(\Xi_c^+ \rightarrow pK^-\pi^+)$ in $p\text{Pb}$ (red triangles) and $\text{Pb}p$ (blue triangles) data samples as a function of p_T . The error bars represent the statistical uncertainties while the squares indicate the systematic uncertainty.

(Italy); GVA, XuntaGal, GENCAT, Inditex, InTalent and Prog. Atracción Talento, CM (Spain); SRC (Sweden); the Leverhulme Trust, the Royal Society, and UKRI (United Kingdom).

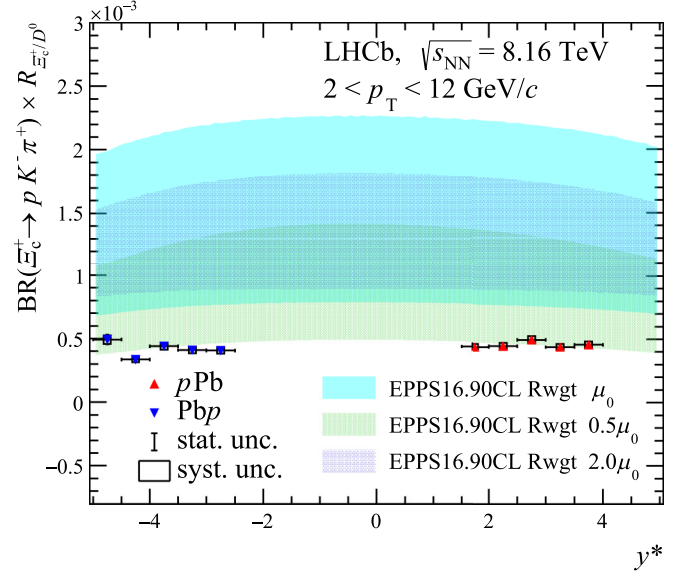


FIG. 10. Production ratio of prompt Ξ_c^+ to D^0 baryons multiplied by $\mathcal{B}(\Xi_c^+ \rightarrow pK^-\pi^+)$ in $p\text{Pb}$ (red triangles) and $\text{Pb}p$ (blue triangles) data samples as a function of y^* . The error bars represent the statistical uncertainties while the squares indicate the systematic uncertainty.

APPENDIX: ADDITIONAL PLOTS

The differential ratios of Ξ_c^+ to Λ_c^+ and to D^0 production multiplied by $\mathcal{B}(\Xi_c^+ \rightarrow pK^-\pi^+)$ are shown in Figs. 7–10 as a function of p_T and y^* .

- [1] R. Aaij *et al.* (LHCb Collaboration), Measurements of prompt charm production cross-sections in pp collisions at $\sqrt{s} = 5$ TeV, *J. High Energy Phys.* **06** (2017) 147.
- [2] J. C. Collins, D. E. Soper, and G. F. Sterman, Heavy particle production in high-energy hadron collisions, *Nucl. Phys. B* **263**, 37 (1986).
- [3] R. Aaij *et al.* (LHCb Collaboration), Measurement of b hadron production fractions in 7 TeV pp collisions, *Phys. Rev. D* **85**, 032008 (2012).
- [4] K. Werner and B. Guiot, Perturbative QCD concerning light and heavy flavor in the EPOS4 framework, *Phys. Rev. C* **108**, 034904 (2023).
- [5] S. Acharya *et al.* (ALICE Collaboration), Λ_c^+ production in pp collisions at $\sqrt{s} = 7$ TeV and in $p\text{-Pb}$ collisions at $\sqrt{s_{\text{NN}}} = 5.02$ TeV, *J. High Energy Phys.* **04** (2018) 108.
- [6] R. Aaij *et al.* (LHCb Collaboration), Prompt Λ_c^+ production in $p\text{Pb}$ collisions at $\sqrt{s_{\text{NN}}} = 5.02$ TeV, *J. High Energy Phys.* **02** (2019) 102.
- [7] H. Albrecht *et al.* (ARGUS Collaboration), Inclusive production of D^0 , D^+ and D^{*+} (2010) mesons in B decays and nonresonant e^+e^- annihilation at 10.6 GeV, *Z. Phys. C* **52**, 353 (1991).
- [8] P. Avery *et al.* (CLEO Collaboration), Inclusive production of the charmed baryon Λ_c^+ from e^+e^- annihilations at $\sqrt{s} = 10.55$ GeV, *Phys. Rev. D* **43**, 3599 (1991).
- [9] S. Chekanov *et al.* (ZEUS Collaboration), Measurement of charm fragmentation ratios and fractions in photoproduction at HERA, *Eur. Phys. J. C* **44**, 351 (2005).
- [10] H. Abramowicz *et al.* (ZEUS Collaboration), Measurement of D^+ and Λ_c^+ production in deep inelastic scattering at HERA, *J. High Energy Phys.* **11** (2010) 009.
- [11] E. Braaten, K.-m. Cheung, S. Fleming, and T. C. Yuan, Perturbative QCD fragmentation functions as a model for heavy quark fragmentation, *Phys. Rev. D* **51**, 4819 (1995).
- [12] S. Acharya *et al.* (ALICE Collaboration), First measurement of Ξ_c^0 production in pp collisions at $\sqrt{s} = 7$ TeV, *Phys. Lett. B* **781**, 8 (2018).
- [13] S. Acharya *et al.* (ALICE Collaboration), Measurement of the cross sections of Ξ_c^0 and Ξ_c^+ baryons and of the branching-fraction ratio $\text{BR}(\Xi_c^0 \rightarrow \Xi^- e^+ \nu_e) / \text{BR}(\Xi_c^0 \rightarrow \Xi^- \pi^+)$ in pp collisions at 13 TeV, *Phys. Rev. Lett.* **127**, 272001 (2021).
- [14] J. R. Christiansen and P. Z. Skands, String formation beyond leading colour, *J. High Energy Phys.* **08** (2015) 003.
- [15] V. Greco and C. M. Ko, Hadronization via coalescence, *Acta Phys. Hung. A* **24**, 235 (2005).
- [16] N. Armesto, Nuclear shadowing, *J. Phys. G* **32**, R367 (2006).
- [17] I. Vitev, Non-Abelian energy loss in cold nuclear matter, *Phys. Rev. C* **75**, 064906 (2007).
- [18] S. Gavin and J. Milana, Energy loss at large x_f in nuclear collisions, *Phys. Rev. Lett.* **68**, 1834 (1992).
- [19] T. Dai, J.-F. Paquet, D. Teaney, and S. A. Bass, Parton energy loss in a hard-soft factorized approach, *Phys. Rev. C* **105**, 034905 (2022).

- [20] M. Wysocki (PHENIX Collaboration), Measurements of cold nuclear matter effects on J/ψ in the PHENIX experiment via deuteron-gold collisions, *J. Phys. G* **35**, 104069 (2008).
- [21] R. Grajcarek, Measurement of heavy-flavor production in Pb-Pb collisions at the LHC with ALICE, *J. Phys.: Conf. Ser.* **420**, 012032 (2013).
- [22] Y.-J. Lee, Quark–gluon droplets engineered, *Nat. Phys.* **15**, 206 (2019).
- [23] J. Rafelski, Strangeness production in the quark gluon plasma, *Nucl. Phys. A* **418**, 215 (1984).
- [24] J. Rafelski, Extreme states of nuclear matter., *Nucl. Phys. A* **374**, 489 (1982).
- [25] P. Koch and J. Rafelski, Time evolution of strange particle densities in hot hadronic matter, *Nucl. Phys. A* **444**, 678 (1985).
- [26] P. Koch, B. Muller, and J. Rafelski, Strangeness in relativistic heavy ion collisions, *Phys. Rep.* **142**, 167 (1986).
- [27] J. Adam *et al.*, Enhanced production of multi-strange hadrons in high-multiplicity proton-proton collisions, *Nat. Phys.* **13**, 535 (2017).
- [28] A. Adare *et al.* (PHENIX Collaboration), Spectra and ratios of identified particles in Au+Au and d +Au collisions at $\sqrt{s_{NN}} = 200$ GeV, *Phys. Rev. C* **88**, 024906 (2013).
- [29] B. I. Abelev *et al.* (STAR Collaboration), Identified baryon and meson distributions at large transverse momenta from Au+Au collisions at $\sqrt{s_{NN}} = 200$ GeV, *Phys. Rev. Lett.* **97**, 152301 (2006).
- [30] R. Aaij *et al.* (LHCb Collaboration), Precision luminosity measurements at LHCb, *JINST* **9**, P12005 (2014).
- [31] R. L. Workman *et al.* (Particle Data Group), Review of particle physics, *Prog. Theor. Exp. Phys.* **2022**, 083C01 (2022).
- [32] A. A. Alves, Jr. *et al.* (LHCb Collaboration), The LHCb detector at the LHC, *JINST* **3**, S08005 (2008).
- [33] R. Aaij *et al.* (LHCb Collaboration), LHCb detector performance, *Int. J. Mod. Phys. A* **30**, 1530022 (2015).
- [34] R. Aaij *et al.*, Performance of the LHCb vertex locator, *JINST* **9**, P09007 (2014).
- [35] P. d’Argent *et al.*, Improved performance of the LHCb outer tracker in LHC Run 2, *JINST* **12**, P11016 (2017).
- [36] M. Adinolfi *et al.*, Performance of the LHCb RICH detector at the LHC, *Eur. Phys. J. C* **73**, 2431 (2013).
- [37] A. A. Alves, Jr. *et al.*, Performance of the LHCb muon system, *JINST* **8**, P02022 (2013).
- [38] R. Aaij *et al.*, The LHCb trigger and its performance in 2011, *JINST* **8**, P04022 (2013).
- [39] T. Sjöstrand, S. Mrenna, and P. Skands, A brief introduction to PYTHIA 8.1, *Comput. Phys. Commun.* **178**, 852 (2008).
- [40] T. Pierog, Iu. Karpenko, J. M. Katzy, E. Yatsenko, and K. Werner, EPOS LHC: Test of collective hadronization with data measured at the CERN Large Hadron Collider, *Phys. Rev. C* **92**, 034906 (2015).
- [41] D. J. Lange, The EvtGen particle decay simulation package, *Nucl. Instrum. Methods Phys. Res. A* **462**, 152 (2001).
- [42] S. Agostinelli *et al.* (Geant4 Collaboration), Geant4: A simulation toolkit, *Nucl. Instrum. Methods Phys. Res. A* **506**, 250 (2003).
- [43] Geant4 Collaboration, J. Allison *et al.*, Geant4 developments and applications, *IEEE Trans. Nucl. Sci.* **53**, 270 (2006).
- [44] G. Dujany and B. Storaci, Real-time alignment and calibration of the LHCb detector in run II, *J. Phys.: Conf. Ser.* **664**, 082010 (2015).
- [45] R. Aaij *et al.*, Tesla: An application for real-time data analysis in High Energy Physics, *Comput. Phys. Commun.* **208**, 35 (2016).
- [46] T. Skwarnicki, A study of the radiative cascade transitions between the Upsilon-prime and Upsilon resonances, PhD thesis, Institute of Nuclear Physics, Krakow, 1986, DESY-F31-86-02.
- [47] M. Pivk and F. R. Le Diberder, sPlot: A statistical tool to unfold data distributions, *Nucl. Instrum. Methods Phys. Res. A* **555**, 356 (2005).
- [48] A. D. Bukin, Fitting function for asymmetric peaks, [arXiv:0711.4449](https://arxiv.org/abs/0711.4449).
- [49] L. Anderlini *et al.*, The PIDCalib package, LHCb-PUB-2016-021, 2016.
- [50] J.-P. Lansberg and H.-S. Shao, Towards an automated tool to evaluate the impact of the nuclear modification of the gluon density on quarkonium, D and B meson production in proton-nucleus collisions, *Eur. Phys. J. C* **77**, 1 (2017).
- [51] A. Kusina, J.-P. Lansberg, I. Schienbein, and H.-S. Shao, Gluon shadowing in heavy-flavor production at the LHC, *Phys. Rev. Lett.* **121**, 052004 (2018).
- [52] A. Kusina, J.-P. Lansberg, I. Schienbein, and H.-S. Shao, Reweighted nuclear PDFs using heavy-flavor production data at the LHC, *Phys. Rev. D* **104**, 014010 (2021).
- [53] H.-S. Shao, HELAC-Onia: An automatic matrix element generator for heavy quarkonium physics, *Comput. Phys. Commun.* **184**, 2562 (2013).
- [54] H.-S. Shao, HELAC-Onia 2.0: An upgraded matrix-element and event generator for heavy quarkonium physics, *Comput. Phys. Commun.* **198**, 238 (2016).
- [55] K. J. Eskola, P. Paakkinen, H. Paukkunen, and C. A. Salgado, EPPS16: Nuclear parton distributions with LHC data, *Eur. Phys. J. C* **77**, 163 (2017).
- [56] LHCb Collaboration, R. Aaij *et al.*, Measurement of the prompt D^0 nuclear modification factor in p Pb collisions at $\sqrt{s_{NN}} = 8.16$ TeV, *Phys. Rev. Lett.* **131**, 102301 (2023).

R. Aaij³², A. S. W. Abdelmotteleb⁵⁰, C. Abellan Beteta⁴⁴, F. Abudinén⁵⁰, T. Ackernley⁵⁴, B. Adeva⁴⁰, M. Adinolfi⁴⁸, P. Adlarson⁷⁷, H. Afsharnia⁹, C. Agapopoulou¹³, C. A. Aidala⁷⁸, Z. Ajaltouni⁹, S. Akar⁵⁹, K. Akiba³², P. Albicocco²³, J. Albrecht¹⁵, F. Alessio⁴², M. Alexander⁵³, A. Alfonso Alberio³⁹, Z. Aliouche⁵⁶, P. Alvarez Cartelle⁴⁹, R. Amalric¹³, S. Amato², J. L. Amey⁴⁸, Y. Amhis^{11,42}, L. An⁴², L. Anderlini²², M. Andersson⁴⁴, A. Andreianov³⁸, M. Andreotti²¹, D. Andreou⁶², D. Ao⁶, F. Archilli^{31,a}, A. Artamonov³⁸, M. Artuso⁶², E. Aslanides¹⁰, M. Atzeni⁴⁴, B. Audurier¹², I. B. Bachiller Perea⁸, S. Bachmann¹⁷, M. Bachmayer⁴³, J. J. Back⁵⁰, A. Bailly-reyre¹³, P. Baladron Rodriguez⁴⁰, V. Balagura¹², W. Baldini^{21,42}, J. Baptista de Souza Leite¹, M. Barbetti^{22,b}, R. J. Barlow⁵⁶, S. Barsuk¹¹, W. Barter⁵², M. Bartolini⁴⁹, F. Baryshnikov³⁸, J. M. Basels¹⁴, G. Bassi^{29,c}, B. Batsukh⁴, A. Battig¹⁵, A. Bay⁴³, A. Beck⁵⁰, M. Becker¹⁵, F. Bedeschi²⁹, I. B. Bediaga¹

- A. Beiter,⁶² S. Belin,⁴⁰ V. Bellee,⁴⁴ K. Belous,³⁸ I. Belov,³⁸ I. Belyaev,³⁸ G. Benane,¹⁰ G. Bencivenni,²³ E. Ben-Haim,¹³ A. Berezhnoy,³⁸ R. Bernet,⁴⁴ S. Bernet Andres,⁷⁶ D. Berninghoff,¹⁷ H. C. Bernstein,⁶² C. Bertella,⁵⁶ A. Bertolin,²⁸ C. Betancourt,⁴⁴ F. Betti,⁴² Ia. Bezshyiko,⁴⁴ S. Bhasin,⁴⁸ J. Bhom,³⁵ L. Bian,⁶⁸ M. S. Bieker,¹⁵ N. V. Biesuz,²¹ P. Billoir,¹³ A. Biolchini,³² M. Birch,⁵⁵ F. C. R. Bishop,⁴⁹ A. Bitadze,⁵⁶ A. Bizzeti,¹ M. P. Blago,⁴⁹ T. Blake,⁵⁰ F. Blanc,⁴³ J. E. Blank,¹⁵ S. Blusk,⁶² D. Bobulska,⁵³ J. A. Boelhauve,¹⁵ O. Boente Garcia,¹² T. Boettcher,⁵⁹ A. Boldyrev,³⁸ C. S. Bolognani,⁷⁴ R. Bolzonella,^{21,d} N. Bondar,^{38,42} F. Borgato,²⁸ S. Borghi,⁵⁶ M. Borsato,¹⁷ J. T. Borsuk,³⁵ S. A. Bouchiba,⁴³ T. J. V. Bowcock,⁵⁴ A. Boyer,⁴² C. Bozzi,²¹ M. J. Bradley,⁵⁵ S. Braun,⁶⁰ A. Brea Rodriguez,⁴⁰ J. Brodzicka,³⁵ A. Brossa Gonzalo,⁴⁰ J. Brown,⁵⁴ D. Brundu,²⁷ A. Buonauro,⁴⁴ L. Buonincontri,²⁸ A. T. Burke,⁵⁶ C. Burr,⁴² A. Bursche,⁶⁶ A. Butkevich,³⁸ J. S. Butter,³² J. Buytaert,⁴² W. Byczynski,⁴² S. Cadeddu,²⁷ H. Cai,⁶⁸ R. Calabrese,^{21,d} L. Calefice,¹⁵ S. Cali,²³ M. Calvi,^{26,e} M. Calvo Gomez,⁷⁶ P. Campana,²³ D. H. Campora Perez,⁷⁴ A. F. Campoverde Quezada,⁶ S. Capelli,^{26,e} L. Capriotti,²⁰ A. Carbone,^{20,f} R. Cardinale,^{24,g} A. Cardini,²⁷ P. Carniti,^{26,e} L. Carus,¹⁴ A. Casais Vidal,⁴⁰ R. Caspary,¹⁷ G. Casse,⁵⁴ M. Cattaneo,⁴² G. Cavallero,^{55,42} V. Cavallini,^{21,d} S. Celani,⁴³ J. Cerasoli,¹⁰ D. Cervenkov,⁵⁷ A. J. Chadwick,⁵⁴ I. C. Chahrouh,⁷⁸ M. G. Chapman,⁴⁸ M. Charles,¹³ Ph. Charpentier,⁴² C. A. Chavez Barajas,⁵⁴ M. Chefdeville,⁸ C. Chen,¹⁰ S. Chen,⁴ A. Chernov,³⁵ S. Chernyshenko,⁴⁶ V. Chobanova,⁴⁰ S. Cholak,⁴³ M. Chrzaszcz,³⁵ A. Chubykin,³⁸ V. Chulikov,³⁸ P. Ciambone,²³ M. F. Cicala,⁵⁰ X. Cid Vidal,⁴⁰ G. Ciezarek,⁴² P. Cifra,⁴² G. Ciullo,^{21,d} P. E. L. Clarke,⁵² M. Clemencic,⁴² H. V. Cliff,⁴⁹ J. Closier,⁴² J. L. Cobbledick,⁵⁶ V. Coco,⁴² J. Cogan,¹⁰ E. Cogneras,⁹ L. Cojocariu,³⁷ P. Collins,⁴² T. Colombo,⁴² L. Congedo,¹⁹ A. Contu,²⁷ N. Cooke,⁴⁷ I. Corredoira,⁴⁰ G. Corti,⁴² B. Couturier,⁴² D. C. Craik,⁴⁴ M. Cruz Torres,^{1,h} R. Currie,⁵² C. L. Da Silva,⁶¹ S. Dadabaev,³⁸ L. Dai,⁶⁵ X. Dai,⁵ E. Dall'Occo,¹⁵ J. Dalseno,⁴⁰ C. D'Ambrosio,⁴² J. Daniel,⁹ A. Danilina,³⁸ P. d'Argent,¹⁹ J. E. Davies,⁵⁶ A. Davis,⁵⁶ O. De Aguiar Francisco,⁵⁶ J. de Boer,⁴² K. De Bruyn,⁷³ S. De Capua,⁵⁶ M. De Cian,⁴³ U. De Freitas Carneiro Da Graca,¹ E. De Lucia,²³ J. M. De Miranda,¹ L. De Paula,² M. De Serio,^{19,i} D. De Simone,⁴⁴ P. De Simone,²³ F. De Vellis,¹⁵ J. A. de Vries,⁷⁴ C. T. Dean,⁶¹ F. Debernardis,^{19,i} D. Decamp,⁸ V. Dedu,¹⁰ L. Del Buono,¹³ B. Delaney,⁵⁸ H.-P. Dembinski,¹⁵ V. Denysenko,⁴⁴ O. Deschamps,⁹ F. Dettori,^{27,j} B. Dey,⁷¹ P. Di Nezza,²³ I. Diachkov,³⁸ S. Didenko,³⁸ L. Dieste Maronas,⁴⁰ S. Ding,⁶² V. Dobishuk,⁴⁶ A. Dolmatov,³⁸ C. Dong,³ A. M. Donohoe,¹⁸ F. Dordei,²⁷ A. C. dos Reis,¹ L. Douglas,⁵³ A. G. Downes,⁸ P. Duda,⁷⁵ M. W. Dudek,³⁵ L. Dufour,⁴² V. Duk,⁷² P. Durante,⁴² M. M. Duras,⁷⁵ J. M. Durham,⁶¹ D. Dutta,⁵⁶ A. Dziurda,³⁵ A. Dzyuba,³⁸ S. Easo,⁵¹ U. Egede,⁶³ V. Egorychev,³⁸ C. Eirea Orro,⁴⁰ S. Eisenhardt,⁵² E. Ejopu,⁵⁶ S. Ek-In,⁴³ L. Eklund,⁷⁷ M. E Elashri,⁵⁹ J. Ellbracht,¹⁵ S. Ely,⁵⁵ A. Ene,³⁷ E. Epple,⁵⁹ S. Escher,¹⁴ J. Eschle,⁴⁴ S. Esen,⁴⁴ T. Evans,⁵⁶ F. Fabiano,^{27,j} L. N. Falcao,¹ Y. Fan,⁶ B. Fang,^{11,68} L. Fantini,^{72,k} M. Faria,⁴³ S. Farry,⁵⁴ D. Fazzini,^{26,e} L. F Felkowski,⁷⁵ M. Feo,⁴² M. Fernandez Gomez,⁴⁰ A. D. Fernez,⁶⁰ F. Ferrari,²⁰ L. Ferreira Lopes,⁴³ F. Ferreira Rodrigues,² S. Ferreres Sole,³² M. Ferrillo,⁴⁴ M. Ferro-Luzzi,⁴² S. Filippov,³⁸ R. A. Fini,¹⁹ M. Fiorini,^{21,d} M. Firlej,³⁴ K. M. Fischer,⁵⁷ D. S. Fitzgerald,⁷⁸ C. Fitzpatrick,⁵⁶ T. Fiutowski,³⁴ F. Fleuret,¹² M. Fontana,¹³ F. Fontanelli,^{24,g} R. Forty,⁴² D. Foulds-Holt,⁴⁹ V. Franco Lima,⁵⁴ M. Franco Sevilla,⁶⁰ M. Frank,⁴² E. Franzoso,^{21,d} G. Frau,¹⁷ C. Frei,⁴² D. A. Friday,⁵³ L. F Frontini,²⁵ J. Fu,⁶ Q. Fuehring,¹⁵ T. Fulghesu,¹³ E. Gabriel,³² G. Galati,^{19,i} M. D. Galati,³² A. Gallas Torreira,⁴⁰ D. Galli,^{20,f} S. Gambetta,^{52,42} M. Gandelman,² P. Gandini,²⁵ Y. Gao,⁷ Y. Gao,⁵ M. Garau,^{27,j} L. M. Garcia Martin,⁵⁰ P. Garcia Moreno,³⁹ J. García Pardiñas,^{26,e} B. Garcia Plana,⁴⁰ F. A. Garcia Rosales,¹² L. Garrido,³⁹ C. Gaspar,⁴² R. E. Geertsema,³² D. Gerick,¹⁷ L. L. Gerken,¹⁵ E. Gersabeck,⁵⁶ M. Gersabeck,⁵⁶ T. Gershon,⁵⁰ L. Giambastiani,²⁸ V. Gibson,⁴⁹ H. K. Gienza,³⁶ A. L. Gilman,⁵⁷ M. Giovannetti,^{23,a} A. Gioventù,⁴⁰ P. Gironella Gironell,³⁹ C. Giugliano,^{21,d} M. A. Giza,³⁵ K. Gizdov,⁵² E. L. Gkougkousis,⁴² V. V. Gligorov,^{13,42} C. Göbel,⁶⁴ E. Golobardes,⁷⁶ D. Golubkov,³⁸ A. Golutvin,^{55,38} A. Gomes,^{1,1} S. Gomez Fernandez,³⁹ F. Goncalves Abrantes,⁵⁷ M. Goncerz,³⁵ G. Gong,³ I. V. Gorelov,³⁸ C. Gotti,²⁶ J. P. Grabowski,⁷⁰ T. Grammatico,¹³ L. A. Granado Cardoso,⁴² E. Graugés,³⁹ E. Graverini,⁴³ G. Graziani,³⁷ L. M. Greeven,³² N. A. Grieser,⁵⁹ L. Grillo,⁵³ S. Gromov,³⁸ B. R. Gruber Cazon,⁵⁷ C. Gu,³ M. Guarise,^{21,d} M. Guittiere,¹¹ P. A. Günther,¹⁷ E. Gushchin,³⁸ A. Guth,¹⁴ Y. Guz,³⁸ T. Gys,⁴² T. Hadavizadeh,⁶³ C. Hadjivasiliou,⁶⁰ G. Haefeli,⁴³ C. Haen,⁴² J. Haimberger,⁴² S. C. Haines,⁴⁹ T. Halewood-leagas,⁵⁴ M. M. Halvorsen,⁴² P. M. Hamilton,⁶⁰ J. Hammerich,⁵⁴ Q. Han,⁷ X. Han,¹⁷ E. B. Hansen,⁵⁶ S. Hansmann-Menzemer,¹⁷ L. Hao,⁶ N. Harnew,⁵⁷ T. Harrison,⁵⁴ C. Hasse,⁴² M. Hatch,⁴² J. He,^{6,m} K. Heijhoff,³² F. H Hemmer,⁴² C. Henderson,⁵⁹ R. D. L. Henderson,^{63,50} A. M. Hennequin,⁵⁸ K. Hennessy,⁵⁴ L. Henry,⁴² J. Herd,⁵⁵ J. Heuel,¹⁴ A. Hicheur,² D. Hill,⁴³ M. Hilton,⁵⁶ S. E. Hollitt,¹⁵ J. Horswill,⁵⁶ R. Hou,⁷ Y. Hou,⁸ J. Hu,¹⁷ J. Hu,⁶⁶ W. Hu,⁵ X. Hu,³ W. Huang,⁶ X. Huang,⁶⁸ W. Hulsbergen,³² R. J. Hunter,⁵⁰ M. Hushchyn,³⁸ D. Hutchcroft,⁵⁴ P. Ibis,¹⁵ M. Idzik,³⁴ D. Ilin,³⁸ P. Ilten,⁵⁹ A. Inglessi,³⁸ A. Iniukhin,³⁸ A. Ishteev,³⁸ K. Ivshin,³⁸ R. Jacobsson,⁴² H. Jage,¹⁴ S. J. Jaimes Elles,⁴¹ S. Jakobsen,⁴² E. Jans,³² B. K. Jashal,⁴¹ A. Jawahery,⁶⁰ V. Jevtic,¹⁵ E. Jiang,⁶⁰ X. Jiang,^{4,6} Y. Jiang,⁶ M. John,⁵⁷ D. Johnson,⁵⁸ C. R. Jones,⁴⁹ T. P. Jones,⁵⁰ B. Jost,⁴² N. Jurik,⁴² I. Juszcak,³⁵ S. Kandybei,⁴⁵ Y. Kang,³ M. Karacson,⁴² D. Karpenkov,³⁸ M. Karpov,³⁸ J. W. Kautz,⁵⁹ F. Keizer,⁴² D. M. Keller,⁶² M. Kenzie,⁵⁰ T. Ketel,³² B. Khanji,¹⁵ A. Kharisova,³⁸ S. Kholodenko,³⁸ G. Khreich,¹¹

- T. Kirn¹⁴, V. S. Kirsebom⁴³, O. Kitouni⁵⁸, S. Klaver³³, N. Kleijne^{29,c}, K. Klimaszewski³⁶, M. R. Kmiec³⁶, S. Koliiev⁴⁶, L. Kolk¹⁵, A. Kondybayeva³⁸, A. Konoplyannikov³⁸, P. Kopciwicz³⁴, R. Kopečna¹⁷, P. Koppenburg³², M. Korolev³⁸, I. Kostiuik³², O. Kot⁴⁶, S. Kotriakhova³⁸, A. Kozachuk³⁸, P. Kravchenko³⁸, L. Kravchuk³⁸, R. D. Krawczyk⁴², M. Kreps⁵⁰, S. Kretzschmar¹⁴, P. Krokovny³⁸, W. Krupa³⁴, W. Krzemien³⁶, J. Kubat¹⁷, S. Kubis⁷⁵, W. Kucewicz³⁵, M. Kucharczyk³⁵, V. Kudryavtsev³⁸, E. K Kulikova³⁸, A. Kupsc⁷⁷, D. Lacarrere⁴², G. Lafferty⁵⁶, A. Lai²⁷, A. Lampis^{27,j}, D. Lancierini⁴⁴, C. Landesa Gomez⁴⁰, J. J. Lane⁵⁶, R. Lane⁴⁸, C. Langenbruch¹⁴, J. Langer¹⁵, O. Lantwin³⁸, T. Latham⁵⁰, F. Lazzari^{29,n}, M. Lazzaroni²⁵, R. Le Gac¹⁰, S. H. Lee⁷⁸, R. Lefèvre⁹, A. Leflat³⁸, S. Legotin³⁸, P. Lenisa^{21,d}, O. Leroy¹⁰, T. Lesiak³⁵, B. Leverington¹⁷, A. Li³, H. Li⁶⁶, K. Li⁷, P. Li⁴², P.-R. Li⁶⁷, S. Li⁷, T. Li⁴, T. Li⁶⁶, Y. Li⁴, Z. Li⁶², X. Liang⁶², C. Lin⁶, T. Lin⁵¹, R. Lindner⁴², V. Lisovskyi¹⁵, R. Litvinov^{27,j}, G. Liu⁶⁶, H. Liu⁶, Q. Liu⁶, S. Liu^{4,6}, A. Lobo Salvia³⁹, A. Loi²⁷, R. Lollini⁷², J. Lomba Castro⁴⁰, I. Longstaff⁵³, J. H. Lopes², A. Lopez Huertas³⁹, S. López Soliño⁴⁰, G. H. Lovell⁴⁹, Y. Lu^{4,o}, C. Lucarelli^{22,b}, D. Lucchesi^{28,p}, S. Luchuk³⁸, M. Lucio Martinez⁷⁴, V. Lukashenko^{32,46}, Y. Luo³, A. Lupato⁵⁶, E. Luppi^{21,d}, A. Lusiani^{29,c}, K. Lynch¹⁸, X.-R. Lyu⁶, R. Ma⁶, S. Maccolini¹⁵, F. Machefert¹¹, F. Maciuc³⁷, I. Mackay⁵⁷, V. Macko⁴³, L. R. Madhan Mohan⁴⁸, A. Maevskiy³⁸, D. Maisuzenko³⁸, M. W. Majewski³⁴, J. J. Malczewski³⁵, S. Malde⁵⁷, B. Malecki^{35,42}, A. Malinin³⁸, T. Maltsev³⁸, G. Manca^{27,j}, G. Mancinelli¹⁰, C. Mancuso^{11,25,q}, R. Manera Escalero³⁹, D. Manuzzi²⁰, C. A. Manzari⁴⁴, D. Marangotto^{25,q}, J. F. Marchand⁸, U. Marconi²⁰, S. Mariani^{22,b}, C. Marin Benito³⁹, J. Marks¹⁷, A. M. Marshall⁴⁸, P. J. Marshall⁵⁴, G. Martelli^{72,k}, G. Martellotti³⁰, L. Martinazzoli^{42,e}, M. Martinelli^{26,e}, D. Martinez Santos⁴⁰, F. Martinez Vidal⁴¹, A. Massafferri¹, M. Materok¹⁴, R. Matev⁴², A. Mathad⁴⁴, V. Matiunin³⁸, C. Matteuzzi²⁶, K. R. Mattioli¹², A. Mauri³², E. Maurice¹², J. Mauricio³⁹, M. Mazurek⁴², M. McCann⁵⁵, L. McConnell¹⁸, T. H. McGrath⁵⁶, N. T. McHugh⁵³, A. McNab⁵⁶, R. McNulty¹⁸, J. V. Mead⁵⁴, B. Meadows⁵⁹, G. Meier¹⁵, D. Melnychuk³⁶, S. Meloni^{26,e}, M. Merk^{32,74}, A. Merli²⁵, L. Meyer Garcia², D. Miao^{4,6}, M. Mikhasenko^{70,r}, D. A. Milanec⁶⁹, E. Millard⁵⁰, M. Milovanovic⁴², M.-N. Minard^{8,s}, A. Minotti^{26,e}, T. Miralles⁹, S. E. Mitchell⁵², B. Mitreska¹⁵, D. S. Mitzel¹⁵, A. Mödden¹⁵, R. A. Mohammed⁵⁷, R. D. Moise¹⁴, S. Mokhnenko³⁸, T. Mombächer⁴⁰, M. Monk^{50,63}, I. A. Monroy⁶⁹, S. Monteil⁹, G. Morello²³, M. J. Morello^{29,c}, M. P. Morgenthaler¹⁷, J. Moron³⁴, A. B. Morris⁴², A. G. Morris⁵⁰, R. Mountain⁶², H. Mu³, E. Muhammad⁵⁰, F. Muheim⁵², M. Mulder⁷³, K. Müller⁴⁴, C. H. Murphy⁵⁷, D. Murray⁵⁶, R. Murta⁵⁵, P. Muzzetto^{27,j}, P. Naik⁴⁸, T. Nakada⁴³, R. Nandakumar⁵¹, T. Nanut⁴², I. Nasteva², M. Needham⁵², N. Neri^{25,q}, S. Neubert⁷⁰, N. Neufeld⁴², P. Neustroev³⁸, R. Newcombe⁵⁵, J. Nicolini^{15,11}, D. Nicotra⁷⁴, E. M. Niel⁴³, S. Nieswand¹⁴, N. Nikitin³⁸, N. S. Nolte⁵⁸, C. Normand^{8,27,j}, J. Novoa Fernandez⁴⁰, G. N Nowak⁵⁹, C. Nunez⁷⁸, A. Oblakowska-Mucha³⁴, V. Obraztsov³⁸, T. Oeser¹⁴, S. Okamura^{21,d}, R. Oldeman^{27,j}, F. Oliva⁵², C. J. G. Onderwater⁷³, R. H. O'Neil⁵², J. M. Otalora Goicochea², T. Ovsianikova³⁸, P. Owen⁴⁴, A. Oyanguren⁴¹, O. Ozcelik⁵², K. O. Padeken⁷⁰, B. Pagare⁵⁰, P. R. Pais⁴², T. Pajero⁵⁷, A. Palano¹⁹, M. Palutan²³, Y. Pan⁵⁶, G. Panshin³⁸, L. Paolucci⁵⁰, A. Papanestis⁵¹, M. Pappagallo^{19,i}, L. L. Pappalardo^{21,d}, C. Pappenheimer⁵⁹, W. Parker⁶⁰, C. Parkes⁵⁶, B. Passalacqua^{21,d}, G. Passaleva²², A. Pastore¹⁹, M. Patel⁵⁵, C. Patrignani^{20,f}, C. J. Pawley⁷⁴, A. Pellegrino³², M. Pepe Altarelli⁴², S. Perazzini²⁰, D. Pereima³⁸, A. Pereiro Castro⁴⁰, P. Perret⁹, K. Petridis⁴⁸, A. Petrolini^{24,g}, A. Petrov³⁸, S. Petrucci⁵², M. Petruzzo²⁵, H. Pham⁶², A. Philippov³⁸, R. Piandani⁶, L. Pica^{29,c}, M. Piccini⁷², B. Pietrzyk⁸, G. Pietrzyk¹¹, M. Pili⁵⁷, D. Pinci³⁰, F. Pisani⁴², M. Pizzichemi^{26,42,e}, V. Placinta³⁷, J. Plews⁴⁷, M. Plo Casasus⁴⁰, F. Polci^{13,42}, M. Poli Lener²³, A. Poluektov¹⁰, N. Polukhina³⁸, I. Polyakov⁴², E. Polcarpo², S. Ponce⁴², D. Popov^{6,42}, S. Poslavskii³⁸, K. Prasanth³⁵, L. Promberger¹⁷, C. Prouve⁴⁰, V. Pugatch⁴⁶, V. Puill¹¹, G. Punzi^{29,n}, H. R. Qi³, W. Qian⁶, N. Qin³, S. Qu³, R. Quagliani⁴³, N. V. Raab¹⁸, B. Rachwal³⁴, J. H. Rademacker⁴⁸, R. Rajagopalan⁶², M. Rama²⁹, M. Ramos Pernas⁵⁰, M. S. Rangel², F. Ratnikov³⁸, G. Raven^{33,42}, M. Rebollo De Miguel⁴¹, F. Redi⁴², J. Reich⁴⁸, F. Reiss⁵⁶, C. Remon Alepuz⁴¹, Z. Ren³, P. K. Resmi⁵⁷, R. Ribatti^{29,c}, A. M. Ricci²⁷, S. Ricciardi⁵¹, K. Richardson⁵⁸, M. Richardson-Slipper⁵², K. Rinnert⁵⁴, P. Robbe¹¹, G. Robertson⁵², A. B. Rodrigues⁴³, E. Rodrigues⁵⁴, E. Rodriguez Fernandez⁴⁰, J. A. Rodriguez Lopez⁶⁹, E. Rodriguez Rodriguez⁴⁰, D. L. Rolf⁴², A. Rollings⁵⁷, P. Roloff⁴², V. Romanovskiy³⁸, M. Romero Lamas⁴⁰, A. Romero Vidal⁴⁰, J. D. Roth^{78,s}, M. Rotondo²³, M. S. Rudolph⁶², T. Ruf⁴², R. A. Ruiz Fernandez⁴⁰, J. Ruiz Vidal⁴¹, A. Ryzhikov³⁸, J. Ryzka³⁴, J. J. Saborido Silva⁴⁰, N. Sagidova³⁸, N. Sahoo⁴⁷, B. Saitta^{27,j}, M. Salomoni⁴², C. Sanchez Gras³², I. Sanderswood⁴¹, R. Santacesaria³⁰, C. Santamarina Rios⁴⁰, M. Santimaria²³, E. Santovetti^{31,a}, D. Saranin³⁸, G. Sarpis¹⁴, M. Sarpis⁷⁰, A. Sarti³⁰, C. Satriano^{30,t}, A. Satta³¹, M. Saur¹⁵, D. Savrina³⁸, H. Sazak⁹, L. G. Scantlebury Smead⁵⁷, A. Scarabotto¹³, S. Schael¹⁴, S. Scherl⁵⁴, M. Schiller⁵³, H. Schindler⁴², M. Schmelling¹⁶, B. Schmidt⁴², S. Schmitt¹⁴, O. Schneider⁴³, A. Schopper⁴², M. Schubiger³², S. Schulte⁴³, M. H. Schune¹¹, R. Schwemmer⁴², B. Sciascia²³, A. Sciuccati⁴², S. Sellam⁴⁰, A. Semennikov³⁸, M. Senghi Soares³³, A. Sergi^{24,g}, N. Serra⁴⁴, L. Sestini²⁸, A. Seuthe¹⁵, Y. Shang⁵, D. M. Shangase⁷⁸, M. Shapkin³⁸, I. Shchemerov³⁸, L. Shchutka⁴³, T. Shears⁵⁴, L. Shekhtman³⁸, Z. Shen⁵, S. Sheng^{4,6}, V. Shevchenko³⁸, B. Shi⁶, E. B. Shields^{26,e}, Y. Shimizu¹¹, E. Shmanin³⁸, R. Shorkin³⁸, J. D. Shupperd⁶², B. G. Siddi^{21,d}, R. Silva Coutinho⁶², G. Simi²⁸, S. Simone^{19,i}, M. Singla⁶³, N. Skidmore⁵⁶, R. Skuza¹⁷

T. Skwarnicki ⁶², M. W. Slater ⁴⁷, J. C. Smallwood ⁵⁷, J. G. Smeaton ⁴⁹, E. Smith ⁴⁴, K. Smith ⁶¹, M. Smith ⁵⁵, A. Snoch ³², L. Soares Lavra ⁹, M. D. Sokoloff ⁵⁹, F. J. P. Soler ⁵³, A. Solomin ^{38,48}, A. Solovov ³⁸, I. Solovyevev ³⁸, R. Song ⁶³, F. L. Souza De Almeida ², B. Souza De Paula ², B. Spaan ^{15,s}, E. Spadaro Norella ^{25,q}, E. Spedicato ²⁰, E. Spiridenkov ³⁸, P. Spradlin ⁵³, V. Sriskaran ⁴², F. Stagni ⁴², M. Stahl ⁴², S. Stahl ⁴², S. Stanislaus ⁵⁷, E. N. Stein ⁴², O. Steinkamp ⁴⁴, O. Stenyakin ³⁸, H. Stevens ¹⁵, S. Stone ^{62,s}, D. Strelalina ³⁸, Y. S. Su ⁶, F. Suljik ⁵⁷, J. Sun ²⁷, L. Sun ⁶⁸, Y. Sun ⁶⁰, P. Svihra ⁵⁶, P. N. Swallow ⁴⁷, K. Swientek ³⁴, A. Szabelski ³⁶, T. Szumlak ³⁴, M. Szymanski ⁴², Y. Tan ³, S. Taneja ⁵⁶, M. D. Tat ⁵⁷, A. Terentev ⁴⁴, F. Teubert ⁴², E. Thomas ⁴², D. J. D. Thompson ⁴⁷, K. A. Thomson ⁵⁴, H. Tilquin ⁵⁵, V. Tisserand ⁹, S. T'Jampens ⁸, M. Tobin ⁴, L. Tomassetti ^{21,d}, G. Tonani ^{25,q}, X. Tong ⁵, D. Torres Machado ¹, D. Y. Tou ³, S. M. Trilov ⁴⁸, C. Trippel ⁴³, G. Tuci ⁶, N. Tuning ³², A. Ukleja ³⁶, D. J. Unverzagt ¹⁷, A. Usachov ³³, A. Ustyuzhanin ³⁸, U. Uwer ¹⁷, A. Vagner ³⁸, V. Vagnoni ²⁰, A. Valassi ⁴², G. Valenti ²⁰, N. Valls Canudas ⁷⁶, M. Van Dijk ⁴³, H. Van Hecke ⁶¹, E. van Herwijnen ⁵⁵, C. B. Van Hulse ^{40,u}, M. van Veghel ³², R. Vazquez Gomez ³⁹, P. Vazquez Regueiro ⁴⁰, C. Vázquez Sierra ⁴², S. Vecchi ²¹, J. J. Velthuis ⁴⁸, M. Veltri ^{22,v}, A. Venkateswaran ⁴³, M. Veronesi ³², M. Vesterinen ⁵⁰, D. Vieira ⁵⁹, M. Vieites Diaz ⁴³, X. Vilasis-Cardona ⁷⁶, E. Vilella Figueras ⁵⁴, A. Villa ²⁰, P. Vincent ¹³, F. C. Volle ¹¹, D. vom Bruch ¹⁰, A. Vorobyev ³⁸, V. Vorobyev ³⁸, N. Voropaev ³⁸, K. Vos ⁷⁴, C. Vrahas ⁵², J. Walsh ²⁹, E. J. Walton ⁶³, G. Wan ⁵, C. Wang ¹⁷, G. Wang ⁷, J. Wang ⁵, J. Wang ⁴, J. Wang ³, J. Wang ⁶⁸, M. Wang ²⁵, R. Wang ⁴⁸, X. Wang ⁶⁶, Y. Wang ⁷, Z. Wang ⁴⁴, Z. Wang ³, Z. Wang ⁶, J. A. Ward ^{50,63}, N. K. Watson ⁴⁷, D. Websdale ⁵⁵, Y. Wei ⁵, B. D. C. Westhenry ⁴⁸, D. J. White ⁵⁶, M. Whitehead ⁵³, A. R. Wiederhold ⁵⁰, D. Wiedner ¹⁵, G. Wilkinson ⁵⁷, M. K. Wilkinson ⁵⁹, I. Williams ⁴⁹, M. Williams ⁵⁸, M. R. J. Williams ⁵², R. Williams ⁴⁹, F. F. Wilson ⁵¹, W. Wislicki ³⁶, M. Witek ³⁵, L. Witola ¹⁷, C. P. Wong ⁶¹, G. Wormser ¹¹, S. A. Wotton ⁴⁹, H. Wu ⁶², J. Wu ⁷, K. Wyllie ⁴², Z. Xiang ⁶, Y. Xie ⁷, A. Xu ⁵, J. Xu ⁶, L. Xu ³, L. Xu ³, M. Xu ⁵⁰, Q. Xu ⁶, Z. Xu ⁹, Z. Xu ⁶, D. Yang ³, S. Yang ⁶, X. Yang ⁵, Y. Yang ⁶, Z. Yang ⁶, Z. Yang ⁶⁰, L. E. Yeomans ⁵⁴, V. Yeroshenko ¹¹, H. Yeung ⁵⁶, H. Yin ⁷, J. Yu ⁶⁵, X. Yuan ⁶², E. Zaffaroni ⁴³, M. Zavertyaev ¹⁶, M. Zdybal ³⁵, M. Zeng ³, C. Zhang ⁵, D. Zhang ⁷, L. Zhang ³, S. Zhang ⁶⁵, S. Zhang ⁶, Y. Zhang ⁵, Y. Zhang ⁵⁷, Y. Zhao ¹⁷, A. Zharkova ³⁸, A. Zhelezov ¹⁷, Y. Zheng ⁶, T. Zhou ⁵, X. Zhou ⁶, Y. Zhou ⁶, V. Zhovkovska ¹¹, X. Zhu ³, X. Zhu ⁷, Z. Zhu ⁶, V. Zhukov ^{14,38}, Q. Zou ^{4,6}, S. Zucchelli ^{20,e}, D. Zuliani ²⁸, and G. Zunica ⁵⁶

(LHCb Collaboration)

¹Centro Brasileiro de Pesquisas Físicas (CBPF), Rio de Janeiro, Brazil

²Universidade Federal do Rio de Janeiro (UFRJ), Rio de Janeiro, Brazil

³Center for High Energy Physics, Tsinghua University, Beijing, China

⁴Institute of High Energy Physics (IHEP), Beijing, China

⁵School of Physics State Key Laboratory of Nuclear Physics and Technology, Peking University, Beijing, China

⁶University of Chinese Academy of Sciences, Beijing, China

⁷Institute of Particle Physics, Central China Normal University, Wuhan, Hubei, China

⁸Université Savoie Mont Blanc, CNRS, IN2P3-LAPP, Annecy, France

⁹Université Clermont Auvergne, CNRS/IN2P3, LPC, Clermont-Ferrand, France

¹⁰Aix Marseille Univ, CNRS/IN2P3, CPPM, Marseille, France

¹¹Université Paris-Saclay, CNRS/IN2P3, IJCLab, Orsay, France

¹²Laboratoire Leprince-Ringuet, CNRS/IN2P3, Ecole Polytechnique, Institut Polytechnique de Paris, Palaiseau, France

¹³LPNHE, Sorbonne Université, Paris Diderot Sorbonne Paris Cité, CNRS/IN2P3, Paris, France

¹⁴I. Physikalisches Institut, RWTH Aachen University, Aachen, Germany

¹⁵Fakultät Physik, Technische Universität Dortmund, Dortmund, Germany

¹⁶Max-Planck-Institut für Kernphysik (MPIK), Heidelberg, Germany

¹⁷Physikalisches Institut, Ruprecht-Karls-Universität Heidelberg, Heidelberg, Germany

¹⁸School of Physics, University College Dublin, Dublin, Ireland

¹⁹INFN Sezione di Bari, Bari, Italy

²⁰INFN Sezione di Bologna, Bologna, Italy

²¹INFN Sezione di Ferrara, Ferrara, Italy

²²INFN Sezione di Firenze, Firenze, Italy

²³INFN Laboratori Nazionali di Frascati, Frascati, Italy

²⁴INFN Sezione di Genova, Genova, Italy

²⁵INFN Sezione di Milano, Milano, Italy

²⁶INFN Sezione di Milano-Bicocca, Milano, Italy

²⁷INFN Sezione di Cagliari, Monserrato, Italy

²⁸Università degli Studi di Padova, Università e INFN, Padova, Padova, Italy

²⁹INFN Sezione di Pisa, Pisa, Italy

- ³⁰INFN Sezione di Roma La Sapienza, Roma, Italy
³¹INFN Sezione di Roma Tor Vergata, Roma, Italy
³²Nikhef National Institute for Subatomic Physics, Amsterdam, Netherlands
³³Nikhef National Institute for Subatomic Physics and VU University Amsterdam, Amsterdam, Netherlands
³⁴AGH - University of Science and Technology, Faculty of Physics and Applied Computer Science, Kraków, Poland
³⁵Henryk Niewodniczanski Institute of Nuclear Physics Polish Academy of Sciences, Kraków, Poland
³⁶National Center for Nuclear Research (NCBJ), Warsaw, Poland
³⁷Horia Hulubei National Institute of Physics and Nuclear Engineering, Bucharest-Magurele, Romania
³⁸Affiliated with an institute covered by a cooperation agreement with CERN
³⁹ICCUB, Universitat de Barcelona, Barcelona, Spain
⁴⁰Instituto Galego de Física de Altas Enerxías (IGFAE), Universidade de Santiago de Compostela, Santiago de Compostela, Spain
⁴¹Instituto de Física Corpuscular, Centro Mixto Universidad de Valencia - CSIC, Valencia, Spain
⁴²European Organization for Nuclear Research (CERN), Geneva, Switzerland
⁴³Institute of Physics, Ecole Polytechnique Fédérale de Lausanne (EPFL), Lausanne, Switzerland
⁴⁴Physik-Institut, Universität Zürich, Zürich, Switzerland
⁴⁵NSC Kharkiv Institute of Physics and Technology (NSC KIPT), Kharkiv, Ukraine
⁴⁶Institute for Nuclear Research of the National Academy of Sciences (KINR), Kyiv, Ukraine
⁴⁷University of Birmingham, Birmingham, United Kingdom
⁴⁸H.H. Wills Physics Laboratory, University of Bristol, Bristol, United Kingdom
⁴⁹Cavendish Laboratory, University of Cambridge, Cambridge, United Kingdom
⁵⁰Department of Physics, University of Warwick, Coventry, United Kingdom
⁵¹STFC Rutherford Appleton Laboratory, Didcot, United Kingdom
⁵²School of Physics and Astronomy, University of Edinburgh, Edinburgh, United Kingdom
⁵³School of Physics and Astronomy, University of Glasgow, Glasgow, United Kingdom
⁵⁴Oliver Lodge Laboratory, University of Liverpool, Liverpool, United Kingdom
⁵⁵Imperial College London, London, United Kingdom
⁵⁶Department of Physics and Astronomy, University of Manchester, Manchester, United Kingdom
⁵⁷Department of Physics, University of Oxford, Oxford, United Kingdom
⁵⁸Massachusetts Institute of Technology, Cambridge, MA, USA
⁵⁹University of Cincinnati, Cincinnati, OH, USA
⁶⁰University of Maryland, College Park, MD, USA
⁶¹Los Alamos National Laboratory (LANL), Los Alamos, NM, USA
⁶²Syracuse University, Syracuse, NY, USA
⁶³School of Physics and Astronomy, Monash University, Melbourne, Australia, associated to⁵⁰
⁶⁴Pontificia Universidade Católica do Rio de Janeiro (PUC-Rio), Rio de Janeiro, Brazil, associated to²
⁶⁵Physics and Micro Electronic College, Hunan University, Changsha City, China, associated to⁷
⁶⁶Guangdong Provincial Key Laboratory of Nuclear Science, Guangdong-Hong Kong Joint Laboratory of Quantum Matter, Institute of Quantum Matter, South China Normal University, Guangzhou, China, associated to³
⁶⁷Lanzhou University, Lanzhou, China, associated to⁴
⁶⁸School of Physics and Technology, Wuhan University, Wuhan, China, associated to³
⁶⁹Departamento de Física, Universidad Nacional de Colombia, Bogota, Colombia, associated to¹³
⁷⁰Universität Bonn - Helmholtz-Institut für Strahlen und Kernphysik, Bonn, Germany, associated to¹⁷
⁷¹Eotvos Lorand University, Budapest, Hungary, associated to⁴²
⁷²INFN Sezione di Perugia, Perugia, Italy, associated to²¹
⁷³Van Swinderen Institute, University of Groningen, Groningen, Netherlands, associated to³²
⁷⁴Universiteit Maastricht, Maastricht, Netherlands, associated to³²
⁷⁵Faculty of Material Engineering and Physics, Cracow, Poland, associated to³⁵
⁷⁶DS4DS, La Salle, Universitat Ramon Llull, Barcelona, Spain, associated to³⁹
⁷⁷Department of Physics and Astronomy, Uppsala University, Uppsala, Sweden, associated to⁵³
⁷⁸University of Michigan, Ann Arbor, MI, United States, associated to⁶²

^aUniversità di Roma Tor Vergata, Roma, Italy.^bUniversità di Firenze, Firenze, Italy.^cScuola Normale Superiore, Pisa, Italy.^dUniversità di Ferrara, Ferrara, Italy.^eUniversità di Milano Bicocca, Milano, Italy.^fUniversità di Bologna, Bologna, Italy.^gUniversità di Genova, Genova, Italy.^hUniversidad Nacional Autónoma de Honduras, Tegucigalpa, Honduras.

ⁱUniversità di Bari, Bari, Italy.

^jUniversità di Cagliari, Cagliari, Italy.

^kUniversità di Perugia, Perugia, Italy.

^lUniversidade de Brasília, Brasília, Brazil.

^mHangzhou Institute for Advanced Study, UCAS, Hangzhou, China.

ⁿUniversità di Pisa, Pisa, Italy.

^oCentral South U., Changsha, China.

^pUniversità di Padova, Padova, Italy.

^qUniversità degli Studi di Milano, Milano, Italy.

^rExcellence Cluster ORIGINS, Munich, Germany.

^sDeceased.

^tUniversità della Basilicata, Potenza, Italy.

^uUniversidad de Alcalá, Alcalá de Henares, Spain.

^vUniversità di Urbino, Urbino, Italy.